Available online at www.sciencedirect.com
ScienceDirect
Advances in Water Resources xxx (2007) xxx–xxx
Advances in Water Resources
www.elsevier.com/locate/advwatres

An external–internal mode coupling for a 3D hydrodynamical model for applications at regional scale (MARS)

Pascal Lazure *, Franck Dumas

Institut Français de Recherche pour l'Exploitation de la Mer, BP 70, 29280 Plouzané, France

Received 2 June 2006; received in revised form 29 June 2007; accepted 29 June 2007

Abstract

This paper presents a 3D model in sigma coordinates. Although the principles it is based on have been established for some time, some original aspects for this type of 3D mode splitting model are presented here. The model was designed to simulate flows in various coastal areas from the regional scale down to the inshore scale of small bays or estuaries where circulation is generally driven by a mix of processes. The processes to be modeled enable simplifications of the Navier–Stokes equations on the classic Boussinesq and hydrostatic hypotheses. These equations are transformed within a sigma framework to make free surface processing easier. The main point of our demonstration focuses on the original aspect of the coupling between barotropic and baroclinic modes especially designed for ADI. It explains how full consistency of the transport calculated within the 2D and 3D equation sets was obtained. Lastly, we describe the physical processes simulated on a realistic configuration at a regional scale in the Bay of Biscay.

Keywords: 3D model; Hydrodynamics; Numerical scheme; Time splitting; Bay of Biscay

1. Introduction

Three-dimensional models have been widely used in coastal ocean modeling activities for two decades now. Most of them solve primitive equations (e.g. Navier–Stokes under the assumptions of Boussinesq and hydrostaticity) because the processes they account for have a horizontal scale which is at least one order of magnitude larger than the vertical one and their time scale is similar to the inertia period.

Up to the early 80s, limited computing power meant that spectral models were widely used [1]. These models used simple turbulence closure schemes and were not well suited to including the one or two equation models required for complex flows. In order to better parameterize turbulence, these models were progressively abandoned and replaced by fully vertical discretized model. From then on, several vertical coordinate systems have been used, with various advantages and drawbacks. Geopotential coordinates (z coordinates system) are used by some ocean models, like OPA [2]. Here, the bottom topography is represented by a series of steps and the bottom boundary layers can be hard to represent in case of steep topographies [3].

Isopycnal coordinate systems consider layers of constant density, as in the Miami Isopycnal Coordinate Model (MICOM) [4]. The advantage is that high resolution is obtained where density gradients are strong. However, applications of such models for shallow water with various stratifications including a well-mixed water column, lead to several difficulties.

For a better description of the bottom and numerical advantages such as a constant number of levels, Phillips [5] introduced normalized depth. This vertical coordinate system, known as terrain-following coordinates, is used by numerous models for both ocean and shelf modeling,

* Corresponding author. Tel.: +33 02 98 22 43 41; fax: +33 02 98 22 48 64.
E-mail address: Pascal.Lazure@ifremer.fr (P. Lazure).

0309-1708/$ - see front matter © 2007 Elsevier Ltd. All rights reserved.
doi:10.1016/j.advwatres.2007.06.010

such as the Princeton Oceanographic Model (POM) [6]. This concept has been extended with generalized topography following coordinates system in order to keep high resolution in the boundary layers of domains including a wide range of water depths (from 10 m to 4000 m) [7,8].

The main drawback of sigma coordinate systems is the computation of the internal pressure gradient, especially over a steep topography [9]. A considerable amount of literature has dealt with the reduction of systematic truncation errors. Shchepetkin and Mac Williams [10] described a new computation of the internal pressure gradient which greatly improves the results for academic configuration, for instance for the seamount problem. This makes the use of terrain-following coordinates models more relevant for coastal dynamics especially in case of steep topography.

Most primitive equation models use time splitting schemes. This aims to solve free surface wave propagation (barotropic mode) and internal motion (internal mode) separately, with time steps that may be different. Because of their high celerity, surface gravity waves require small time steps to be properly solved through explicit numerical schemes, whereas internal waves with weaker celerity may be processed with larger time steps. The two modes are closely linked as the barotropic pressure gradient calculated with the external mode is prescribed to the internal mode. On the other hand, the bottom stress, integrated pressure gradient and internal stresses are provided to the external mode. This theoretical procedure engenders clearly identified problems due to the use of different schemes which have their own time steps. Continuity equations must be fulfilled by both modes consistently, i.e. the vertically integrated 3D velocity field must be identical to that of barotropic velocity. Usually, the internal mode time stepping uses an implicit resolution of the vertical derivative needed to accurately describe boundary layers which require high vertical resolution. Most of the differences between 3D free surface models concern the external time stepping.

External mode resolution can be divided into two parts: explicit and semi-implicit or implicit models. Explicit schemes are used by the most popular models: Coherens [11], POM [12] and ROMS [13]. In that case, the ratio between internal and external time steps is around 10–50. However, for stability reasons, the terms given to the external mode usually need to be re-evaluated during an internal time step.

Implicit or semi-implicit resolution of the external mode, allows large time steps, because it is no longer limited by the CFL (Courant–Friedrichs–Levy) condition, and in that case, the external and internal time steps are usually equal. The ECOMsi [14] semi-implicit version of POM uses Casulli and Cheng's [15] semi-implicit method for the barotropic mode. Three-dimensional models using a semi-implicit method (ADI) to solve the barotropic mode have been described recently [16,17,8]. They use the same time step for both internal and external modes and therefore do not require any re-evaluation of the coupling term during temporal integration.

Most of the models apply a correction to the 3D predicted currents to ensure consistency. This corrector step consists in adding to the 3D predicted currents the local difference between the 2D (external mode) calculated currents and the vertical integration of the predicted 3D currents. This simple method is used by most of the models like POM and HYCOM and as Pietrzak et al. [8] noted, they work properly. ROMS uses a more sophisticated approach. The vertically averaged velocity of the baroclinic mode is corrected by a filter applied to every external time step [13,18].

A different method was proposed by Lin and Falconer [16]. The barotropic and baroclinic modes using the same time step, a first prediction is performed to obtain the free surface gradient. The 3D field is integrated and the bottom stress and momentum correction factors are then computed. A second step is performed by the 2D mode with these new parameters and a new 3D integration is achieved with the new free surface field.

An original method was recently proposed by Chen [19]. A free surface correction method (FSC) is used to obtain consistency between modes (i.e. locally and globally mass conservative). It involves two steps: the first leads to an intermediate free surface which is corrected within the second step by a semi-implicit method. It has been shown to be unconditionally stable with respect to gravity waves.

This method and the former ones, even the simplest of them, are mass conservative, both locally and globally. However, they involve a corrective step which is more or less sophisticated. At the end of the internal time step, the 3D horizontal velocity being solved, the complete consistency is not fully achieved. Whatever the type of correction and the way it occurs, the correction step does not involve the momentum equation and therefore has no physical signification. This can, in theory, induce spurious effects that are very hard to quantify.

This paper aims to present a 3D model based on an ADI scheme for the barotropic mode. In order to eliminate problems induced by the use of different schemes for the internal mode, external mode equations were rewritten to allow strictly identical discretization over both time and space for the internal mode. It focuses on the coupling between modes. An iterative procedure is used to provide full consistency between modes without any extra correction.

After presenting the equations, the coupling procedure is described step by step. Some other numerical considerations and an optimization of the iterative process are then given. To illustrate the ability of the model to reproduce various coastal processes, a realistic application to the Bay of Biscay is presented.

2. Equations

The set of equations solved has long been known. Details can be found in Blumberg and Mellor [12], amongst others. Here, we shall simply provide a reminder that the

Please cite this article in press as: Lazure P, Dumas F, An external–internal mode coupling for a 3D hydrodynamical ..., Adv Water Resour (2007), doi:10.1016/j.advwatres.2007.06.010

hypotheses under which these equations (so called primitive equations) are obtained are classic approximations:

- that of Boussinesq: density in the medium slightly deviates from a reference density called ρ_0 and therefore can be replaced by a reference density except within the gravity term,
- the hydrostatic approximation resulting from scaling the equations: the horizontal movement scale is assumed to be an order of magnitude larger that the vertical one.

Equations are presented here in a sigma coordinate framework:

$$\sigma = \frac{z+H}{\zeta+H} \tag{1}$$

with σ is the vertical coordinate, $H(x,y)$ is the absolute value of bottom position, $\zeta(x,y)$ is the sea surface elevation. z and sigma increase upwards. The result is that at the sea surface $(z=\zeta)\sigma=1$ and at the sea floor $(z=-H)\sigma=0$.

In addition, we introduced the following notation make the writing of any advection term simpler:

$$L(A) = u\frac{\partial A}{\partial x} + v\frac{\partial A}{\partial y} + w^*\frac{\partial A}{\partial \sigma} \tag{2}$$

where w^* is the vertical velocity in the sigma coordinate framework (x,y,σ) whereas w is the vertical velocity in the physical framework (x,y,z). It reads:

$$w^* = \frac{1}{D}\left(w - \sigma\frac{\partial\zeta}{\partial t} - u\left(\sigma\frac{\partial\zeta}{\partial x} + (\sigma-1)\frac{\partial H}{\partial x}\right) - v\left(\sigma\frac{\partial\zeta}{\partial y} + (\sigma-1)\frac{\partial H}{\partial y}\right)\right) \tag{3}$$

where $D(x,y)$ is the height of water column, $D = H + \zeta$.

The set of primitive equations is then in Cartesian coordinates:

$$\frac{1}{D}\frac{\partial p}{\partial \sigma} = -\rho g \tag{4}$$

$$\frac{\partial\zeta}{\partial t} + \frac{\partial Du}{\partial x} + \frac{\partial Dv}{\partial y} + \frac{\partial Dw^*}{\partial \sigma} = 0 \tag{5}$$

$$\frac{\partial u}{\partial t} + L(u) - fv = -g\frac{\partial\zeta}{\partial x} - \frac{1}{\rho_0}\frac{\partial Pa}{\partial x} + \pi_x + \frac{1}{D}\frac{\partial\left(\frac{nz}{D}\frac{\partial u}{\partial\sigma}\right)}{\partial\sigma} + F_x \tag{6}$$

$$\frac{\partial v}{\partial t} + L(v) + fu = -g\frac{\partial\zeta}{\partial y} - \frac{1}{\rho_0}\frac{\partial Pa}{\partial y} + \pi_y + \frac{1}{D}\frac{\partial\left(\frac{nz}{D}\frac{\partial v}{\partial\sigma}\right)}{\partial\sigma} + F_y \tag{7}$$

with x,y,σ is the cartesian coordinates of the framework; u,v,w^* are the zonal, meridian and vertical velocity components; P_a is the atmospheric pressure at sea surface; $f = 2\Omega\sin\phi$ is the Coriolis parameter; $\Omega = 2\pi/86164\ \mathrm{rad\ s^{-1}}$ is the earth's rotation frequency; g is the gravity; $\rho = \rho(S,T,p)$ is the seawater density; p is the pressure; ρ_0 is the reference density; nz is the vertical eddy viscosity; v_x and v_y are the horizontal eddy viscosity coefficients.

Zonal and meridian components of the baroclinic pressure gradient are noted from above on (π_x,π_y).

The transport of any dissolved matter is solved in a mass conservative form giving:

$$\frac{\partial DTr}{\partial t} + \frac{\partial D(uTr - k_x\frac{\partial Tr}{\partial x})}{\partial x} + \frac{\partial D(vTr - k_y\frac{\partial Tr}{\partial y})}{\partial y} + \frac{\partial D(w^*Tr - \frac{kz}{D^2}\frac{\partial Tr}{\partial\sigma})}{\partial\sigma} = \mathrm{Sources} - \mathrm{Sinks} \tag{8}$$

where Tr stands for any tracer: temperature, salinity, any dissolved tracers; *Sources* are the sources of tracer Tr; *Sinks* are the sinks of tracer Tr; kz is the vertical eddy diffusivity; k_x and k_y are the horizontal eddy diffusivity coefficients.

To properly close the system, the equation of state relates density to salinity, temperature and pressure:

$$\rho = G(S,T,p) \tag{9}$$

Function G is not stated explicitly here. It is either linearized around point $(T_0,S_0,p=0)$ for very shallow areas or fully developed as Mellor [20] does for deeper waters.

From the Eq. (1) and introducing the buoyancy $b = -g(\rho-\rho_0)/\rho_0$ within a sigma coordinate framework, the terms (π_x,π_y) read:

$$\pi_x = \frac{\partial}{\partial x}\left[D\int_\sigma^1 b\,\mathrm{d}\sigma\right] + b\left(\sigma\frac{\partial D}{\partial x} - \frac{\partial H}{\partial x}\right) \tag{10}$$

$$\pi_y = \frac{\partial}{\partial y}\left[D\int_\sigma^1 b\,\mathrm{d}\sigma\right] + b\left(\sigma\frac{\partial D}{\partial y} - \frac{\partial H}{\partial y}\right) \tag{11}$$

Horizontal friction term:

$$F_x = \frac{1}{D}\frac{\partial}{\partial x}\left[Dv_x\frac{\partial u}{\partial x}\right] + \frac{1}{D}\frac{\partial}{\partial x}\left[v_x\left(\frac{\partial H}{\partial x} - \sigma\frac{\partial D}{\partial x}\right)\frac{\partial u}{\partial\sigma}\right] + \frac{1}{D}\frac{\partial}{\partial\sigma}\left[v_x\left(\frac{\partial H}{\partial x} - \sigma\frac{\partial D}{\partial x}\right)\frac{\partial u}{\partial x}\right] + \frac{1}{D}\frac{\partial}{\partial\sigma}\left[\frac{v_x}{D}\left(\frac{\partial H}{\partial x} - \sigma\frac{\partial D}{\partial x}\right)^2\frac{\partial u}{\partial\sigma}\right] \tag{12}$$

$$F_y = \frac{1}{D}\frac{\partial}{\partial y}\left[Dv_y\frac{\partial v}{\partial y}\right] + \frac{1}{D}\frac{\partial}{\partial y}\left[v_y\left(\frac{\partial H}{\partial y} - \sigma\frac{\partial D}{\partial y}\right)\frac{\partial v}{\partial\sigma}\right] + \frac{1}{D}\frac{\partial}{\partial\sigma}\left[v_y\left(\frac{\partial H}{\partial y} - \sigma\frac{\partial D}{\partial y}\right)\frac{\partial v}{\partial y}\right] + \frac{1}{D}\frac{\partial}{\partial\sigma}\left[\frac{v_y}{D}\left(\frac{\partial H}{\partial y} - \sigma\frac{\partial D}{\partial y}\right)^2\frac{\partial v}{\partial\sigma}\right] \tag{13}$$

The horizontal turbulent diffusion operators are not written in a fully discretized form, but simplified according to Mellor [21]. This approximation is relatively acceptable, as long as the discretized vertical layers cross the isopycns smoothly, i.e. in the case of a smooth bathymetry gradient. In most of application, the two components of horizontal eddy viscosity are set equal to a constant v. This leads to:

Please cite this article in press as: Lazure P, Dumas F, An external–internal mode coupling for a 3D hydrodynamical ..., Adv Water Resour (2007), doi:10.1016/j.advwatres.2007.06.010

$$F_x = \frac{\partial}{\partial x}\left(v\frac{\partial u}{\partial x}\right) + \frac{\partial}{\partial y}\left(v\frac{\partial u}{\partial y}\right), \quad F_y = \frac{\partial}{\partial x}\left(v\frac{\partial v}{\partial x}\right) + \frac{\partial}{\partial y}\left(v\frac{\partial v}{\partial y}\right) \tag{14}$$

The flux at the upper and lower boundaries of the domain together with kinematic conditions leads to the following sets of equations:

Boundary conditions at the surface $\sigma = 1$	Boundary conditions at the bottom $\sigma = 0$
$\frac{nz}{D}\frac{\partial u}{\partial \sigma} = \frac{\tau_{sx}}{\rho_0}$	$\frac{nz}{D}\frac{\partial u}{\partial \sigma} = \frac{\tau_{bx}}{\rho_0}$
$\frac{nz}{D}\frac{\partial v}{\partial \sigma} = \frac{\tau_{sy}}{\rho_0}$	$\frac{nz}{D}\frac{\partial v}{\partial \sigma} = \frac{\tau_{by}}{\rho_0}$
$\frac{kz}{D}\frac{\partial T}{\partial \sigma} = \frac{Q_T}{\rho_0 C_p}$	$kz\frac{\partial T}{\partial \sigma} = 0$
$kz\frac{\partial S}{\partial \sigma} = 0$	$kz\frac{\partial S}{\partial \sigma} = 0$
$w^* = 0$	$w^* = 0$

where Q_T is the heat flux at the air–sea interface; $(\tau_{sx}, \tau_{sy}) = \rho_a Cd_S \|\vec{W}\|(W_x, W_y)$ are the surface stress components; $\rho_a = 1.25\ \mathrm{kg/m^3}$ is the air density; $Cd_S = 0.016$ is the surface drag coefficient; (W_x, W_y) is the wind velocity vector at 10 m above the sea surface; $(\tau_{bx}, \tau_{by}) = \rho_0 Cd_B \|\vec{u}\|(u, v)$ are the bottom stress components with $Cd_B = \left(\frac{\kappa}{\ln\left(\frac{z+H+z_0}{z_0}\right)}\right)^2$ where κ refers to the Von Karman constant and z_0 the bed roughness.

2.1. Turbulence closure

The most often used closure scheme in coastal ocean models at present are the two-equation closure model that follows the k–kl theory assumptions [22] and the k-epsilon ones. The transport equation for turbulent kinetic energy, k, in most turbulent models used for geophysical flows is expressed as follows:

$$\frac{\partial k}{\partial t} + L(k) = \frac{1}{D}\frac{\partial\left(\frac{nz}{s_k D}\frac{\partial k}{\partial \sigma}\right)}{\partial \sigma} + \mathrm{Prod} + \mathrm{Dest} - \varepsilon \tag{15}$$

where s_k stands for the turbulence Schmidt number for k and Prod and Dest are respectively the production by velocity shear and the destruction by buoyancy. They are expressed in the following manner:

$$\mathrm{Prod} = nz\left[\left(\frac{\partial u}{\partial z}\right)^2 + \left(\frac{\partial v}{\partial z}\right)^2\right] \quad \text{and} \quad \mathrm{Dest} = -kz\frac{\partial b}{\partial z} \tag{16}$$

Finally, ε is the dissipation rate. The second equation for the dissipation rate ε requires many more assumptions. We prefer to replace it here by the relation following the k–ε approximation described and tested by Luyten [23]

$$\varepsilon = \varepsilon_0 \frac{k^{3/2}}{l} \tag{17}$$

where the mixing length is $l = \kappa z_*(1 - z_*/H)$, z_* stands for the distance to the bottom and ε_0 is determined for an equilibrium neutral flow near a wall: its value is $\varepsilon_0 = 0.166$.

The eddy coefficients are expressed as

$$nz = S_m k^{\frac{1}{2}} l + nz_{\mathrm{bg}} \quad \text{and} \quad kz = S_T k^{\frac{1}{2}} l + kz_{\mathrm{bg}} \tag{18}$$

where S_m and S_T are stability functions and nz_{bg} and kz_{bg} refer to background viscosity and diffusivity.

2.2. Barotropic mode equations

The mode splitting approach leads to build a specific barotropic model by integrating the Eqs. (5)–(7) over the vertical from bottom ($\sigma = 0$) to top ($\sigma = 1$) and considering kinematic boundary conditions. It gives the following set of equations:

$$\frac{\partial \zeta}{\partial t} + \frac{\partial D\bar{u}}{\partial x} + \frac{\partial D\bar{v}}{\partial y} = 0 \tag{19}$$

$$\frac{\partial \bar{u}}{\partial t} = -g\frac{\partial \zeta}{\partial x} - \frac{1}{\rho_0}\frac{\partial Pa}{\partial x} + \frac{1}{\rho_0 D}(\tau_{sx} - \tau_{bx}) + \int_0^1 [fv - L(u) + \pi_x + F_x]\mathrm{d}\sigma \tag{20}$$

$$\frac{\partial \bar{v}}{\partial t} = -g\frac{\partial \zeta}{\partial y} - \frac{1}{\rho_0}\frac{\partial Pa}{\partial y} + \frac{1}{\rho_0 D}(\tau_{sy} - \tau_{by}) + \int_0^1 [-fu - L(v) + \pi_y + F_y]\mathrm{d}\sigma \tag{21}$$

where the mean current over depth is defined as

$$(\bar{u}, \bar{v}) = \int_0^1 (u, v)\mathrm{d}\sigma \tag{22}$$

3. Coupling of barotropic and baroclinic modes

3.1. Time stepping

The time stepping used to solve the barotropic mode is an Alternate Direction Implicit (hereafter noted ADI) scheme. It was described in the early 70s [24,25]. Wolf [26] compared ADI to a fully explicit scheme in a series of various situations, from test cases to realistic simulation of the southern North Sea. Since then, it has been used by Lin and Falconer [16] and more recently by Pietrzak et al. [8]. Both its drawbacks and advantages are well known. On the one hand, the external gravity wave term which is coded semi-implicitly removes the most stringent stability criterion ($\Delta t < \Delta x/\sqrt{gD}$), giving the model better stability. In practice, this allows larger time steps than that resulting from the criterion. On the other hand, increasing the time step too far beyond the explicit limit results in damping of the barotropic mode.

The ADI method is only implicit with respect to the direction of the computation. Thus, the free surface elevation is calculated every half time step, whereas $\bar{u}$ and $\bar{v}$ are calculated alternatively. Computation of $\bar{u}$ and ζ are performed in a row-wise manner whereas $\bar{v}$ and ζ computations are

Please cite this article in press as: Lazure P, Dumas F, An external–internal mode coupling for a 3D hydrodynamical ..., Adv Water Resour (2007), doi:10.1016/j.advwatres.2007.06.010

performed in column-wise. This means that the set of Eqs. (6), (19) and (20) is solved at a given time step and the set 7, 19 and 21 will be solved a half time step later. The use of a spatially centered second order scheme and the staggered Arakawa C grid lead to a tridiagonal linear system being solved using LU factorization. Special attention was paid to the discretization of the advection operators which was based on the efficient schemes given by Leonard [27,28].

3.2. Discretization

The indexes i, j, k refer to the position in the x, y, σ direction. The free surface elevation ζ is located at the center of the horizontal grid. The zonal velocity u is calculated at the same latitude as ζ and is shifted by half a longitudinal grid size dx. The velocity located on the right side (to the East) of ζ keeps the same i index, while the nearest velocity point located on the western side of ζ is referred to as $i-1$. The same rule is applied for the meridian velocity v. The point of v calculation of ζ nearest to the North is located at the same longitude and has the same index, j. The following variables are located at the center of each mesh and have thus the same i,j indexes: ζ: free surface elevation, C: concentration of any tracer (temperature or salinity included), D_ζ: water depth at ζ position (e.g. $D_\zeta = H + \zeta$), kz,nz: eddy diffusivity and viscosity, k: turbulent kinetic energy, w_z^*: vertical velocity in sigma coordinates. The following variables are located at the same position as $u : \bar{u}$: zonal barotropic velocity, H_u: the reference water depth, D_u: height of the whole water column that is to say $D_u = H_u + 0.5(\zeta_{i,j} + \zeta_{i+1,j})$. The following variables are located at the same position as v:$\bar{v}$: meridian barotropic velocity, H_v: the reference water depth, D_v: water depth. This gives three different depth informations (namely D_ζ, D_u, D_v) for each grid cell.

The vertical discretization is also performed according to a staggered grid. The vertical location of each value at the center of the grid is referred to as the k index and is located at σ_k from the bottom ($\sigma = 0$) up to the surface ($\sigma = 1$). The next mesh center is referred to as $k+1$ and is located at σ_{k+1}. At σ_k the following variables are calculated: C: concentration of tracers, S salinity, T temperature and ρ density. Both velocity components u and v are calculated at σ_k. At the middle of these two cells, the vertical velocity calculation point has the index k and is located at $\sigma w_k = 0.5 * (\sigma_k + \sigma_{k+1})$. The following variables are calculated at the same horizontal location as ς and at σw_k: kz,nz: eddy diffusivity and viscosity, k: turbulent kinetic energy, w^*: vertical velocity in sigma coordinate.

3.3. Rewriting depth-integrated equations

The resolution of the external mode is not based on the classical Saint-Venant equations (obtained by integrating 3D equations using Leibniz's rule together with surface and bottom cinematic conditions) but from the set of Eqs. (19)–(21). Let k be the vertical index varying from 1 at the bottom up to $k$max at the surface; thus $k$max is the number of vertical levels. Each vertical level is located at σ_k. Let $\Delta\sigma_k = \frac{\sigma_{k+1} - \sigma_{k-1}}{2}$ represents the thickness of the level k. From each side of the boundaries, we define $\sigma_0 = -\sigma_1$ and $\sigma_{k\max+1} = 2 - \sigma_{k\max}$. It is easy to check that: $\sum_{k=1}^{k\max} \Delta\sigma_k = 1$.

In order to simplify notation of Eqs. (20) and (21), we define the following discretized terms of their right-hand side:

$$G_u = \sum_{k=1}^{k\max} (fvz_k - L(uz_k) + \pi_{xk} + F_{xk})\Delta\sigma_k + \frac{\tau_{sx}}{\rho_0 D_u} - \frac{\tau_{bx}}{\rho_0 D_u} - \frac{1}{\rho_0}\frac{\partial P_a}{\partial x} \tag{23}$$

$$G_v = \sum_{k=1}^{k\max} (-fuz_k - L(vz_k) + \pi_{yk} + F_{yk})\Delta\sigma_k + \frac{\tau_{sy}}{\rho_0 D_v} - \frac{\tau_{by}}{\rho_0 D_v} - \frac{1}{\rho_0}\frac{\partial P_a}{\partial y} \tag{24}$$

And the barotropic velocities coming out Eqs. (20) and (21) are computed as

$$\bar{u} = \sum_{k=1}^{k\max} uz_k \Delta\sigma_k, \quad \bar{v} = \sum_{k=1}^{k\max} vz_k \Delta\sigma_k \tag{25}$$

uz_k and vz_k stands for the value of u et v at sigma level k.

3.4. Time stepping scheme and coupling procedure

To focus on the time derivative and the model's kernel, we will not describe the spatial derivatives, but will now describe a step of the $\bar{u}$, ζ and uz computation. Transposition to the other velocity component could then be easily inferred. As the coupling is based on an iterative predictor–corrector, we introduce the following notations:

$\zeta^n, \bar{u}^n, uz^n$: sea surface elevation, barotropic and 3D zonal component of velocity at time step n.
$\zeta^{n+\frac{1}{2}}, \bar{v}^{n+\frac{1}{2}}, vz^{n+\frac{1}{2}}$: sea surface elevation, barotropic and 3D meridional component of velocity at time step $n + 1/2$ which corresponds to dt/2 time after time step n.
$\zeta^l, \bar{u}^l, uz^l$: estimation at iteration l of predictor–corrector of sea surface elevation, barotropic and 3D zonal component of velocity at time step $n+1$.

The algorithm is shown in Fig. 1. Considering that all variables are known at time n and $n + 1/2$, the iterative process is built on the following steps:

Step 1: barotropic forwarding (first iteration).

Eqs. (19) and (20) are time differenced as follows:

$$\frac{\zeta^l - \zeta^{n+\frac{1}{2}}}{0.5\Delta t} + \left(\frac{\partial(D_u^{n+1/2}\bar{u}^l)}{\partial x}\right) = -\left(\frac{\partial\left(D_v^{n+1/2}\bar{v}^{n+1/2}\right)}{\partial y}\right) \tag{26}$$

$$\frac{\bar{u}^l - \bar{u}^n}{\Delta t} + \alpha_\varsigma g\left(\frac{\partial\zeta^l}{\partial x}\right) = -\mathrm{Snlt}(uz_k^n) + \mathrm{Shdt}(uz_k^n) + \mathrm{bst}(uz_k^n) + \mathrm{RCT}(\zeta^n, vz_k^{n+\frac{1}{2}}, b_k^{n+\frac{1}{2}}) \tag{27}$$

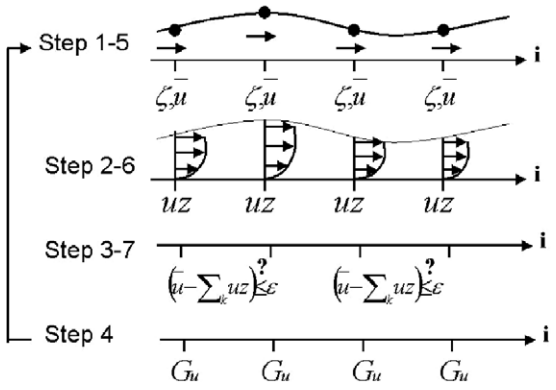

Fig. 1. Barotropic–baroclinic mode fitting.

The right-hand side of the last equation is composed of the following terms:

Non-linear terms:

$$\mathrm{Snlt}(uz_k^l) = \sum_{k=1}^{k\max} \mathrm{nlt}(uz_k^l)\Delta\sigma_k \quad \text{where:}$$

$$\mathrm{nlt}(uz_k^l) = uz_k^l \frac{\partial uz_k^l}{\partial x} + vz_k^{n+1/2} \frac{\partial uz_k^n}{\partial y} + \overline{w^{n+\frac{1}{2}} \frac{\partial uz^l}{\partial \sigma}} \tag{28}$$

The asterisk has been omitted for the w expression and will be omitted hereafter. The bar over the expression $w\partial u/\partial\sigma$ means that this quantity is evaluated at σw_k and σw_{k-1} and interpolated at σ_k. We note that the cross derivative ($\frac{\partial}{\partial y}$ for a row-wise manner computation) will not take part in the iterative process.

Horizontal diffusion terms:

$$\mathrm{Shdt}(uz_k^l) = \sum_{k=1}^{k\max} \mathrm{hdt}(uz_k^l)\Delta\sigma_k \quad \text{where:}$$

$$\mathrm{hdt}(uz_k^l) = \nu\left(\frac{\partial^2 uz_k^l}{\partial x^2} + \frac{\partial^2 uz_k^n}{\partial y^2}\right) \tag{29}$$

As for non-linear terms, the cross derivative does not take part in the iterative process.

Bottom friction term:

$$\mathrm{bst}(uz^l) = \frac{Cd_B uz_k^l \sqrt{(uz_k^n)^2 + (vz_k^{n+1/2})^2}}{D_u^{n+1/2}} \tag{30}$$

The terms remaining constant over the iterative process have been gathered in:

$$\mathrm{RCT}(\zeta^n, vz_k^{n+\frac{1}{2}}, bz_k^{n+\frac{1}{2}}) = -(1-\alpha_\zeta) g \frac{\partial \zeta^n}{\partial x} + \sum_{k=1}^{k\max} (fvz_k^{n+1/2} + \pi_k^{n+1/2})\Delta\sigma_k + \frac{\tau_{sx}^{n+1/2}}{\rho_0 D_u^{n+1/2}} - \frac{1}{\rho_0}\frac{\partial Pa^{n+1/2}}{\partial x} \tag{31}$$

Parameter α_ς is an implicitation factor: in cases where it is set equal to 1, the free surface elevation is taken to be fully implicit along each line. The set of equations is solved at the same time for the entire line. At the end of the first step, a predicted new free surface elevation and average velocity are obtained along the line. The internal pressure gradient $\pi_k^{n+1/2}$ is calculated by Shchepetkin [10] algorithm designed to minimize errors due to the use of sigma coordinate over steep bathymetry.

Step 2: transect updating (first iteration).

The predicted free surface allows the uz_k on the transect to be predicted. Time differencing considers all vertical derivatives as being implicit. At point (i,j) (for the sake of simplicity, indexes i and j are omitted hereafter) Eq. (20) is discretized as

$$\frac{uz_k^l - uz_k^n}{\Delta t} - \frac{1}{(D_u^{n+1/2})^2}\left[\frac{\partial\left(nz^{n+1/2}\frac{\partial uz^l}{\partial\sigma}\right)}{\partial\sigma}\right]_k + \overline{w^{n+1/2}\frac{\partial uz^l}{\partial\sigma}} = -g\left(\alpha_\zeta\frac{\partial\zeta^l}{\partial x} + (1-\alpha_\zeta)\frac{\partial\zeta^n}{\partial x}\right) + \pi_k^{n+1/2} + fvz_k^{n+1/2} - \mathrm{nlt}(uz_k^n) + \mathrm{hdt}(uz_k^n) \tag{32}$$

At that point, the right-hand side is known. This leads to a tridiagonal matrix which is easily solved at each point i along the line, giving rise to a predicted value of uz_k^l along the transect.

Step 3: convergence evaluation (each iteration).

This step consists of the convergence assessment of the iterative process. Convergence is reached when for any point i along row j the following criterion is satisfied:

$$\left|\bar{u}^l - \sum_{k=1}^{k\max} uz_k^l \Delta\sigma_k\right| < \varepsilon \tag{33}$$

ε is a tolerance value introduced in order to account for the precision of real value coding in IEEE norm. It is set to 10^{-5} m s^{-1} being a trade off value between single precision coding and the irrelevance of weaker current departure.

Whenever the convergence is not obtained at every point of the line j being computed, the iterative process goes ahead to the next line (increment of j and restart to step 1). As long as the criterion is not satisfied for any point the process goes on step 4.

Step 4: new assessment of the right-hand side (second and following iterations).

The right-hand side (RHS) of Eq. (27) is re-assessed by introducing three implicitation factors (one for the bottom stress expression, one for non-linear terms and another for horizontal diffusion) in order to properly center all these terms in time.

$$Gu_k^l = -\alpha_{\mathrm{nl}}\mathrm{Snlt}(uz_k^l) + \alpha_{\mathrm{hd}}\mathrm{Shdt}(uz_k^l) + \alpha_{\mathrm{bs}}\mathrm{bst}(uz_k^l) - (1-\alpha_{\mathrm{nl}})\mathrm{Snlt}(uz_k^n) + (1-\alpha_{\mathrm{hd}})\mathrm{Shdt}(uz_k^n) + (1-\alpha_{\mathrm{bs}})\mathrm{bst}(uz_k^n) + \mathrm{RCT}(\zeta^n, vz_k^{n+\frac{1}{2}}, b_k^{n+\frac{1}{2}}) \tag{34}$$

Step 5: new free surface prediction (second and following iterations).

This step is similar to step 1 with a new assessment of RHS:

Please cite this article in press as: Lazure P, Dumas F, An external–internal mode coupling for a 3D hydrodynamical ..., Adv Water Resour (2007), doi:10.1016/j.advwatres.2007.06.010

$$\frac{\zeta^{l+1}-\zeta^{n+\frac{1}{2}}}{0.5\Delta t}+\left(\frac{\partial(D_u^{n+1/2}\bar{u}^{l+1})}{\partial x}\right)=-\left(\frac{\partial(D_v^{n+1/2}\bar{v}^{n+1/2})}{\partial y}\right) \quad (35)$$

$$\frac{\bar{u}^{l+1}-\bar{u}^{n}}{\Delta t}+\alpha_\varsigma g\left(\frac{\partial\zeta}{\partial x}\right)^{l+1}=Gu_k^l \quad (36)$$

At this stage, the resolution of these two equations will give a new evaluation of $\bar{u}$ and ζ.

Step 6: new transect velocity evaluation (second and following iteration).

This step is similar to step 2, except for the two implicitation factors:

$$\begin{aligned}\frac{uz_k^{l+1}-uz_k^n}{\Delta t}&-\frac{1}{(D_u^{n+1/2})^2}\left[\frac{\partial\left(nz^{n+1/2}\frac{\partial uz^{l+1}}{\partial\sigma}\right)}{\partial\sigma}\right]+\overline{w^{n+\frac{1}{2}}\frac{\partial uz^l}{\partial\sigma}}\\&=-g\left(\alpha_\varsigma\frac{\partial\zeta^{l+1}}{\partial x}+(1-\alpha_\varsigma)\frac{\partial\zeta^n}{\partial x}\right)+\pi_k^{n+1/2}+\mathrm{fvz}_k^{n+1/2}\\&\quad-\alpha_{\mathrm{nl}}\mathrm{nltu}(uz_k^l)+\alpha_{\mathrm{hd}}\mathrm{hdt}(uz_k^l)-(1-\alpha_{\mathrm{nl}})\mathrm{nltu}(uz_k^n)\\&\quad+(1-\alpha_{\mathrm{hd}})\mathrm{hdt}(uz_k^n)\end{aligned} \quad (37)$$

Then the process goes to step 3 for a new assessment of the convergence criterion.

3.5. Computational cost

The barotropic ADI resolution (Eqs. (26), (27), (35), (36)) for the given *j*th line leads to a linear tridiagonal system which evolves all along the predictor corrector iterative process. But modifications from one iteration to another are highly localized within a part of the right-hand side of the system. That means the lower–upper (LU) factorization is performed only once until the convergence is reached. The resolution at each iteration consists in updating the right-hand side (RHS) vector; this is done by splitting this RHS into two parts: one explicit and one implicit. This could be written formally in the following way:

$$\begin{pmatrix} b_{1,j} & c_{1,j} & 0 & \cdots & 0\\ a_{2,j} & b_{2,j} & c_{2,j} & \ddots & 0\\ 0 & \ddots & \ddots & \ddots & 0\\ \vdots & \ddots & \ddots & \ddots & c_{n-1,j}\\ 0 & \cdots & 0 & a_{n,j} & b_{n,j}\end{pmatrix}\begin{pmatrix} u_{1,j}\\ \zeta_{2,j}\\ \vdots\\ \zeta_{\mathrm{imax}-1,j}\\ u_{\mathrm{imax}-1,j}\end{pmatrix} = \begin{pmatrix} y_{1,j}\\ y_{2,j}\\ \vdots\\ y_{n-1,j}\\ y_{n,j}\end{pmatrix}^{\exp}+\begin{pmatrix} y_{1,j}\\ y_{2,j}\\ \vdots\\ y_{n-1,j}\\ y_{n,j}\end{pmatrix}^{\mathrm{imp}} \quad (38)$$

into which imax is the number of computational grid cells in the row direction. The coefficient dependencies of this linear system may be written as

$$a_{l,j}=f_a(g,\Delta t,\Delta x,D_u^{n+\frac{1}{2}}) \quad (39)$$

$$b_{l,j}=1 \quad (40)$$

$$c_{l,j}=f_c(g,\Delta t,\Delta x,D_u^{n+\frac{1}{2}}) \quad (41)$$

$$y_{l,j}^{\exp}=f_{y\exp}\left(Pa,W,uz^n,vz^{n+\frac{1}{2}},T^{n+\frac{1}{2}},S^{n+\frac{1}{2}},\zeta^l,w^{n+\frac{1}{2}},nz^{n+\frac{1}{2}}\right) \quad (42)$$

$$y_{l,j}^{\mathrm{imp}}=f_{y\mathrm{imp}}(uz^l,\zeta^l) \quad (43)$$

where index *j* stands for the number of the given grid line discretized here. This is because *a*,*b*,*c* vectors, like the vector $y^{\exp}$ and odd components of vector y^{imp} (i.e. those related to ζ) do not evolve over iterations. So, after the first iteration the computations are significantly lighter, simply updating the even components of y^{imp} and solving the bidiagonal (one upper and one lower) linear systems.

For 3D mode, the computation consists in a series of 1D vertical models at each *u*-location. The way these equations are discretized gives a set of tridiagonal linear systems like

$$\begin{pmatrix} bz_{i,j,1} & cz_{i,j,1} & 0 & \cdots & 0\\ az_{i,j,2} & bz_{i,j,2} & cz_{i,j,2} & \ddots & 0\\ 0 & \ddots & \ddots & \ddots & 0\\ \vdots & \ddots & \ddots & \ddots & cz_{i,j,k\max-1}\\ 0 & \cdots & 0 & az_{i,j,k\max} & bz_{i,j,k\max}\end{pmatrix}\begin{pmatrix} uz_{i,j,1}\\ uz_{i,j,2}\\ \vdots\\ uz_{i,j,k\max-1}\\ uz_{i,j,k\max}\end{pmatrix} = \begin{pmatrix} yz_{i,j,1}\\ yz_{i,j,2}\\ \vdots\\ yz_{i,j,k\max-1}\\ yz_{i,j,k\max}\end{pmatrix}^{\exp}+\begin{pmatrix} yz_{i,j,1}\\ yz_{i,j,2}\\ \vdots\\ yz_{i,j,k\max-1}\\ yz_{i,j,k\max}\end{pmatrix}^{\mathrm{imp}} \quad (44)$$

where indexes *i* and *j* stand for the coordinates of the point u in the computational grid. The dependencies of the linear system are here the following:

$$az_{i,j,k}=f_{az}(nz^{n+\frac{1}{2}},\Delta\sigma_k,D_u^{n+\frac{1}{2}},w_{k-1}^{n+\frac{1}{2}}) \quad (45)$$

$$bz_{i,j,k}=f_{bz}(nz^{n+\frac{1}{2}},\Delta\sigma_k,D_u^{n+\frac{1}{2}},w_k^{n+\frac{1}{2}},w_{k-1}^{n+\frac{1}{2}}) \quad (46)$$

$$cz_{i,j,k}=f_{cz}(nz^{n+\frac{1}{2}},\Delta\sigma_k,D_u^{n+\frac{1}{2}},w_k^{n+\frac{1}{2}}) \quad (47)$$

$$yz_{i,j,k}^{\exp}=f_{yz\exp}(Pa,W,uz^n,vz^{n+\frac{1}{2}},T^{n+\frac{1}{2}},S^{n+\frac{1}{2}},\zeta^n) \quad (48)$$

$$yz_{i,j,k}^{\mathrm{imp}}=f_{yz\mathrm{imp}}(uz^l,\zeta^l) \quad (49)$$

This is processed in exactly the same way as for the barotropic mode through an LU factorization and storage performed once and for all (because the $az_{i,j,k}$, $bz_{i,j,k}$, $cz_{i,j,k}$ vectors remain constant over successive iterations) and full updating of the implicit part of the RHS. The computation cost is again higher for the first iteration than for the following ones.

Please cite this article in press as: Lazure P, Dumas F, An external–internal mode coupling for a 3D hydrodynamical ..., Adv Water Resour (2007), doi:10.1016/j.advwatres.2007.06.010

4. Other numerical considerations

This paragraph briefly describes the next step to achieve the updating of all state variables. We focus on few, less classic points, such as river introduction, time step optimization and limitation.

4.1. Other steps

Once the horizontal velocity components $\bar{u}$ and uz and the sea level elevations have been calculated, the vertical velocity over the whole domain is calculated by a vertical integration of Eq. (7).

Next, the salinity and temperature and eventually dissolved tracers are calculated with a classic time integration scheme used in most 3D models. The vertical derivative of each constituent is considered as being implicit to allow large time steps with a high vertical refinement. For the salinity calculation, the boundary condition in each estuary is described in the following paragraph. Horizontal advection resolution uses the QUICKEST scheme [28]. Density is then updated according to Mellor [20] state equation.

TKE is calculated, also using a scheme very similar to that for the tracers and eddy viscosity and diffusivity are updated according to Eq. (18).

All variables being updated, the time is increased by half a time step as required by the ADI scheme. The boundary conditions at open sea, surface and estuary are read (or calculated in process studies) and a new iteration begins. The horizontal velocities $\bar{v}$ and vz and the elevation are calculated in column-wise manner in the same way as was described in Section 3.

4.2. River introduction

The river runoff Q is introduced as a source term in the vertically integrated continuity Eq. (19) written at the input point:

$$\frac{\partial \zeta}{\partial t}+\frac{\partial D\bar{u}}{\partial x}+\frac{\partial D\bar{v}}{\partial y}=\frac{Q}{\text{surf}} \tag{50}$$

where surf stands for the grid cell surface. After the barotropic–baroclinic iterative adjustment process, w is assessed predictively throughout the local continuity equation which is integrated from bottom to the top as

$$Dw(\sigma)=Dw(0)-\frac{\partial \zeta}{\partial t}-\int_0^{\sigma}\left(\frac{\partial Du}{\partial x}+\frac{\partial Dv}{\partial y}\right)\mathrm{d}\sigma' \tag{51}$$

where $w(0)=0$. We can easily check that at the top $w=-\frac{Q}{\text{Surf}\times D}$ in the grid cell of input. It simply states that at each half time step a corresponding amount of fresh water is poured from the surface into the estuary. For salinity calculations, the resolution of the salinity is computed in the estuary as everywhere in the domain. The input of salt in the estuary which is obviously nil leads to a decrease of salinity in local and adjacent grid cells (due to advection) which corresponds exactly to the amount of fresh water inputs. For any other tracers in the river, the amount of matter introduced in the estuary is simply: $C\cdot w$ where C is the concentration in fresh water.

4.3. Stability

The stability ADI scheme used for hydrodynamic coastal models has been studied by Leendertsee [25]. His analysis was carried out from a simplified system of the barotropic equations neglecting all the non-linear terms (from advection to bottom friction) and the Coriolis force. Thus the system is reduced to a set of oscillating equations of dimensions 3 (u,v,ζ). He showed that the three eigenmodes of the system are always stable through an ADI discretization. Their amplification factor modulus is either 1 in the case where the CFL criterion for external gravity waves is fulfilled or lower than 1 when this Courant number exceeds 1, meaning a damping of these free oscillating solutions. Thus, Leendertsee showed ADI to be an unconditionally stable scheme for external gravity waves.

The Saint-Venant equations (that drives the barotropic mode) system to solve is not as simple as the one studied by Lendertsee, insofar as there is extra coupling between equations through the Coriolis force and non-linearities with the advection terms or the bottom dissipation. Noting that perturbations mostly appear within the advection terms and are dissipated by the bottom friction, Leendertsee [29] carried out a stability study based on the equation which accounts for advection and dissipation by the bottom friction in a one-dimensional problem:

$$\frac{\partial u}{\partial t}+u\frac{\partial u}{\partial x}+\frac{C_d|\vec{u}|u}{H}=0 \tag{52}$$

He looks at the behavior of the solution of the form $u=u_0\mathrm{e}^{\mathrm{i}(\omega t+kx)}$ into various types of discretization of this equation by calculating the amplification factor of the solution $\lambda=\frac{u_j^{t+\Delta t}}{u_j^t}$.

It can easily be established that the amplification of the explicitly discretized

$$u_j^{t+\Delta t}-u_j^t+\frac{\Delta t}{2\Delta x}u_j^t(u_{j+1}^t-u_{j-1}^t)+\frac{C_d\Delta t|u|}{H}u_j^t=0 \tag{53}$$

is

$$\lambda=1+\frac{C_d}{H}\Delta t|u|-\mathrm{i}\frac{|u|\Delta t}{\Delta x}\sin(kx) \tag{54}$$

where i stands for the imaginary complex unit and j for the index in the x direction. This fully explicit discretization is unconditionally unstable because $|\lambda|>1$ for any time and space step. We can now look at the more general equation solved within the model, in which the Coriolis force and external pressure gradient have been removed and horizontal diffusion included:

$$\frac{\partial u}{\partial t}+u\frac{\partial u}{\partial x}+\frac{C_d|\vec{u}|u}{H}=v\frac{\partial^2 u}{\partial x^2} \tag{55}$$

Please cite this article in press as: Lazure P, Dumas F, An external–internal mode coupling for a 3D hydrodynamical ..., Adv Water Resour (2007), doi:10.1016/j.advwatres.2007.06.010

which is discretized in MARS according to

$$\begin{aligned} & u_j^{t+\Delta t} - u_j^t \\ & + \frac{\Delta t}{2\Delta x} u_j^t \left[\alpha_{\mathrm{nl}} u_j^{t+\Delta t} (u_{j+1}^{t+\Delta t} - u_{j-1}^{t+\Delta t}) + (1-\alpha_{\mathrm{nl}}) u_j^t (u_{j+1}^t - u_{j-1}^t) \right] \\ & + \frac{C_d \Delta t |u|}{H} [\alpha_{\mathrm{bs}} u_j^{t+\Delta t} + (1-\alpha_{\mathrm{bs}}) u_j^t] \\ & - v \left[\alpha_{\mathrm{hd}} \frac{u_{j+1}^{t+\Delta t} - 2u_j^{t+\Delta t} + u_{j-1}^{t+\Delta t}}{\Delta x^2} + (1-\alpha_{\mathrm{hd}}) \frac{u_{j+1}^t - 2u_j^t + u_{j-1}^t}{\Delta x^2} \right] \\ & = 0 \end{aligned} \tag{56}$$

The general analysis of this scheme leads to the amplification factor

$$\lambda = \frac{1 - (1-\alpha_{\mathrm{bs}}) \frac{C_d \Delta t |u|}{H} + (1-\alpha_{\mathrm{hd}}) \frac{2v\Delta t}{\Delta x^2} (\cos(kx) - 1) - \mathrm{i}(1-\alpha_{\mathrm{nl}}) \frac{|u|\Delta t}{\Delta x} \sin(kx)}{1 + \alpha_{\mathrm{bs}} \frac{C_d \Delta t |u|}{H} - \alpha_{\mathrm{hd}} \frac{2v\Delta t}{\Delta x^2} (\cos(kx+\omega t) - 1) + \mathrm{i}\alpha_{\mathrm{nl}} \frac{|u|\Delta t}{\Delta x} \sin(kx+\omega t)} \tag{57}$$

where $(\alpha_{\mathrm{nl}}, \alpha_{\mathrm{hd}}, \alpha_{\mathrm{bs}})$ is the triplet of implicitation factors of Eq. (34) in which each element is in [0: 1]. This form enables the behavior of the scheme to be discussed, depending on how we account for the various terms (e.g. their rate of implicitation).

Looking at the various terms one by one, we recover some well-known results:

- the fully implicit advection ($\alpha_{\mathrm{nl}} = 1$) is unconditionally stable whereas a fully explicit one is constrained by $\mathrm{CFL} = \frac{u\Delta t}{\Delta x} \leqslant 1$
- the fully implicit horizontal diffusion ($\alpha_{\mathrm{hd}} = 1$) is unconditionally unstable whereas the fully explicit is conditionally stable with $\frac{v\Delta t}{\Delta x^2} \leqslant 1$
- the implicit part of the bottom stress is unconditionally stable whereas its explicit part is stable up to: $\frac{C_d \Delta t |u|}{H} \leqslant 2$

It is very difficult to analyze the general case in its full complexity because it gives a series of equilibria that may vary from place to place in realistic applications where hydrodynamic conditions (depths and currents) are highly variable. Below, we carefully examine the equilibrium between the advection and the bottom dissipation. As shown above, a fully explicit discretization of the Eq. (52) leads to an unconditionally unstable scheme. From the general expression of the amplification factor, the stability criterion analysis comes in four sets of implicitation factors summarized in Table 1.

In the best case, which is having all terms time-centered, the criterion for a classical bottom drag coefficient ($C_{\mathrm{d}} = 2.10^{-3} usi$) may be written as $\mathrm{CFL} \leqslant 1.6 \times 10^{-2} \frac{\Delta x}{H}$. Getting Courant numbers close to 1 implies having a ratio grid step over depth equal to 60, which is clearly too restrictive for the set of applications we aimed at dealing with. The horizontal dissipation term is used to dampen spurious oscillations. As we can see in the analytical form of the amplification factor, it is more efficient to use it as being fully explicit despite the fact that it is not centered in time, thus decaying the scheme's order of approximation. Practically speaking, the implicitation factor α_{hd} is adjustable, knowing that it should be set to 0.5 for the sake of precision and to 0 for stability considerations.

The regular set of parameters is chosen as $(\alpha_{\mathrm{nl}}, \alpha_{\mathrm{hd}}, \alpha_{bs}) = (0.5, 0.5, 1.0)$. The choice of the implicitation factor for the bottom friction is linked to the one of the vertical dissipation scheme as a boundary condition of this operator. This operator is processed in a fully implicit manner for stability considerations thus giving a fully implicit bottom stress. Finally, in order to properly close the set of parameter values, it is reminded that the implicitation factor of the external pressure gradient here noted α_ζ is set to 0.5 as recommended by Leendertsee [25].

Table 1
Stability criterion according to implicitation factors

$(\alpha_{\mathrm{nl}}, \alpha_{\mathrm{bs}})$	(0,0)	(1,1)	(0,0.5)	(0.5,0.5)
Stability condition	Unconditionally unstable	Unconditionally stable	$\frac{\Delta t \lvert u\rvert}{\Delta x} \leqslant \frac{2C_d \Delta x}{H}$	$\frac{\Delta t \lvert u\rvert}{\Delta x} \leqslant \frac{8C_d \Delta x}{H}$

The number and the various space scales processes allow an empirical criterion based on the model's behavior in realistic conditions to be exhibited and a two order time-centered scheme to be sought (i.e. all implicitation factors set to 0.5) which is

$$\mathrm{CFL} = \frac{u_{\max} \Delta t}{\Delta x} \leqslant C_{\mathrm{crit}}, \quad \text{where } C_{\mathrm{crit}} = 0.7$$

It is first worth noticing that the barotropic model is coupled with a 3D model. The coupling method described in Section 3 shows that the time discretization of the equations of the barotropic mode are the same as that discussed by Lendertsee [25] with an external pressure gradient split into two parts so that the operator is centered in time and a fully implicit treatment of the mass conservation integrated equation. All the other terms are centered in time, as we have seen just above, for the non-linear terms but also for the horizontal dissipation terms. On the vertical, a fully implicit scheme ensures that we will not be limited by the fast vertical diffusion processes. The lack of influence on vertical diffusion terms on stability has also been outlined by De Goede [30] in a somewhat similar time splitting method.

Finally the dynamic equations are solved together with a transport equation used to compute salinity and temperature field changes. These transport equations are coupled with the dynamic equation through the buoyancy and must be solved in a way consistent with the mass conservation

Please cite this article in press as: Lazure P, Dumas F, An external–internal mode coupling for a 3D hydrodynamical ..., Adv Water Resour (2007), doi:10.1016/j.advwatres.2007.06.010

solver in order to be mass preserving, not only for water but also for any tracer. This equation is discretized with an explicit one step forward in the time scheme for which a classic CFL limitation compatible with the empirical criterion expressed above must be fulfilled.

4.4. Computational cost and convergence

This prediction–correction approach has been tested for a long time in a wide range of configurations. This has provided good empirical knowledge of its behavior with respect to stability and convergence for complex realistic cases being all highly non-linear. First, the iterative process converges with a small number of iterations: between 1 and 10, at worst. The convergence speed is of course governed by the tolerance previously noted as ε. The lower the tolerance, the greater the number of iterations will be.

Fig. 2 shows the average (over the whole lines) number of iterations and the computational cost normalized by the one of a single iteration computation (dashed line) with respect to the tolerance ε. These curves were obtained with the implementation of MARS for the realistic application presented in Section 5.

The average number of iteration increases with the decreasing of the tolerance but the convergence is reached for all the grid cells within an acceptable number of iteration (i.e. less than four iterations) even for very weak current authorized departure ($0.01\ \mathrm{mm\ s^{-1}}$). Above this precision the number of iteration rises dramatically because of inadequate computer precision. An increase in this parameter to higher values lowers the number of iterations almost linearly. At the extreme, when this value was on the order of the maximum current, a single iteration is performed.

The computational cost curve shows that each additional iteration has a cost of only 25% of the first one due to computational savings by storing LU factorizations and frozen RHS terms through the iterative process (see Section 3.5).

Despite these features were plotted for a particular application (see Section 5), they are relevant of the general behavior of the model which convergence is reached in any case within a maximum of ten iterations. This, in addition with the cost of a single extra iteration, provides us with a very efficient system able to match without any post-correction step barotropic and baroclinic modes.

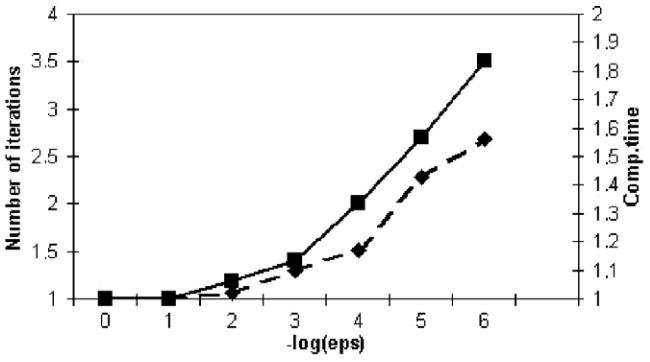

Fig. 2. number of iterations (full line) computational cost (dashed line) versus precision criterion. Computational cost is expressed as the ratio of CPU time over CPU time for the first iteration.

4.5. Time step optimization

In order to reduce computational time, the time step was periodically adjusted to fit the critical CFL insofar as possible. During a typical duration of two semidiurnal tidal cycles (25 h) the criterion was assessed at each time step. At the end of this observation time, the time step was increased by 20% when C_{crit} had never been reached. Conversely, the time step was reduced to fit 80% of the critical criterion if it was exceeded. The period of observation was used to avoid time step variations which could follow the tidal cycle. It allowed a larger time step during neap tide or weak wind conditions and a reduced time step during spring tide or storm conditions. It is limited, for reasons, not of stability but to fully solve short period phenomenon as for example in the presented application the shallow water non-linearly generated tidal component M4.

Each time the time step is modified, the integration is not time-centered. Several comparisons between fixed and adjusted time steps have shown that the increase in truncation errors induced by non-time centered time steps which arises as Δt is modified, has no significant effects because the time step adjustment is performed only once per observing period (i.e. once every 24 h).

4.6. On-going developments

The MARS model is highly modular. The iterative procedure leads to a spatial and temporal discretization which enables other numerical schemes to be tested simply. For example, the non-linear horizontal terms discretization which is centered in the momentum equation can be relatively simply discretized according to a high order scheme.

Current developments concern a higher level turbulence closure scheme. The generalized two equation turbulence scheme [31] is being included in the model.

Although a high order scheme [10] is used to calculate the internal pressure gradient, the simple sigma coordinate system is known to generate spurious currents over steep topography and especially over the shelf break. Therefore, integration of a generalized sigma coordinate [7] is being developed and a first analysis has shown that this system is fully compatible with the iterative procedure described.

Lastly, a downscaling procedure has been implemented in the model. This is based on the AGRIF package [32] and allows the different embedded domains of increasing resolutions to be dealt with during the same run. The one-way coupling (from the large model to the smaller one) is currently operational. The two-way coupling has yielded preliminary results but is still under development to ensure that it works correctly in various situations.

Please cite this article in press as: Lazure P, Dumas F, An external–internal mode coupling for a 3D hydrodynamical ..., Adv Water Resour (2007), doi:10.1016/j.advwatres.2007.06.010

5. Realistic simulations: application to the bay of Biscay

The sole aim of this application is to show the model's ability to reproduce both hydrodynamic and hydrological structures accurately. For this purpose, we present here an application in the Bay of Biscay with a special focus on the continental shelf. Realistic simulations were performed in order to validate the model through comparisons with surveys.

5.1. Context

A wide range of physical processes takes place in the Bay of Biscay [33]:

- The tide is semidiurnal. The tide at Brest varies from 3 m during neap tides up to 7 m during spring tides. Tidal amplitude decreases slightly southwards. Tidal currents show strong spatial gradients: strong in the northern part of the Bay, they decrease southwardly to become weak to very weak south of 48°N [34].
- Wind-induced currents are greatly variable but show seasonal trends. During fall and winter, winds blow from the SW and create a poleward flow [34], whereas during spring and summer, winds blow from the NW [35] and induce a SW flow in the surface layer.
- Puillat et al. [35] presented most of the surveys made in the past ten years over the French continental shelf. The weak tidal mixing over the shelf and in the deep ocean gives rise to thermal stratification during spring and summer. This strong stratification isolates a cold pool on the shelf (i.e., between isobath 50 m and 150 m) which is characterized by a temperature of about 12 °C throughout the year. North winds induce upwelling along the coast of the Landes; westerly to north-westerly winds are likely to induce local upwelling south of Brittany [35]. Tidal-induced mixing generates thermal fronts off Brittany around Ushant Island [36,37].
- Runoff from three major rivers, the Loire, Gironde and Adour, bring large amounts of fresh water into the Bay of Biscay. Their average discharges are 900 m^3/s for the first two and 250 m^3/s for the last one; they peak during winter and spring and lower at the end of spring to reach their minimum at the end of summer. The salinity patterns are highly variable as shown recently by Puillat [35].

Although we focused on time scales ranging from a few days to several years, tides must still be fully resolved because of their role in mixing and frontogenesis and potential long-term transport through tidal residual currents. The first simulation dedicated to validating the tidal dynamics is outlined.

Very few current measurements are available for the continental shelf of the Bay of Biscay. An ADCP, including a pressure sensor, was moored off the Brittany coast, 20 km NW of Belle Ile island over a depth of 68 m [38]. A comparison of sea level elevation and current 20 m above the sea bed is shown. Finally, the model results have been summarized for comparison with observed hydrological structures: a local upwelling in southern Brittany in June 1997 and a surface salinity plume in April 1998 indicated by surveys [35].

5.1.1. Model configurations

A 3D model has been built on a domain which extends in longitude from the French coast to 8°W and in latitude from the Spanish coast to 49°N (Fig. 3). The bathymetry was provided by the SHOM (Hydrological and Oceanographic Service of the French Navy). It has a grid size of 5 km. This model is used to describe hydrodynamics over decades. It gets 30 sigma levels. To reproduce hydrological features in the surface layer, the sigma level distribution is denser near the surface. The model uses open boundary conditions calculated by a larger barotropic model.

5.1.2. Boundary conditions

A wider barotropic model extending from Portugal to Iceland was used to provide boundary conditions for the three-dimensional model. Tidal constituents along the open boundary of the large model were extracted from the Schwiderski atlas [39]. Surface wind stress and pressure were provided by the ARPEGE model from Meteo France. This model has a spatial resolution of 0.5° in longitude and latitude and provides four analyzed wind and pressure fields a day. The 3D model was forced by the free surface elevation and a zero normal gradient condition was used for the velocity along the open boundary.

Surface heat fluxes were calculated with bulk formulae [40] which involve wind speed, air temperature, nebulosity and relative humidity. The first parameter was provided by the meteorological model, while climatology values were used for the three other variables. Temperature and salinity at the open boundary were taken from Reynaud's Climatology [41].

Loire, Gironde and Adour river runoffs are prescribed in their own estuaries and taken from daily measurements.

5.1.3. Initial conditions

Currents were considered to be equal to zero at the beginning of the simulation and the free surface elevation was interpolated in the domain from values at the open boundary conditions. The spin-up time for tidal dynamics and any gravity waves is very short due to their high velocity: its order of magnitude was 5 days in that configuration. The salinity was chosen to be homogenous and equal to 35.5 psu and the temperature chosen was equal to 11 °C over the whole domain. This thermal structure over the shelf is close to that recorded during winter. That is why simulations began at that time (in our case on 01/01/1996).

In the first application, no attention was paid to initializing complex thermal structures in the deep Bay because we focused on the shelf hydrodynamics. As shown by several theoretical works and observation reviewed by

Please cite this article in press as: Lazure P, Dumas F, An external–internal mode coupling for a 3D hydrodynamical ..., Adv Water Resour (2007), doi:10.1016/j.advwatres.2007.06.010

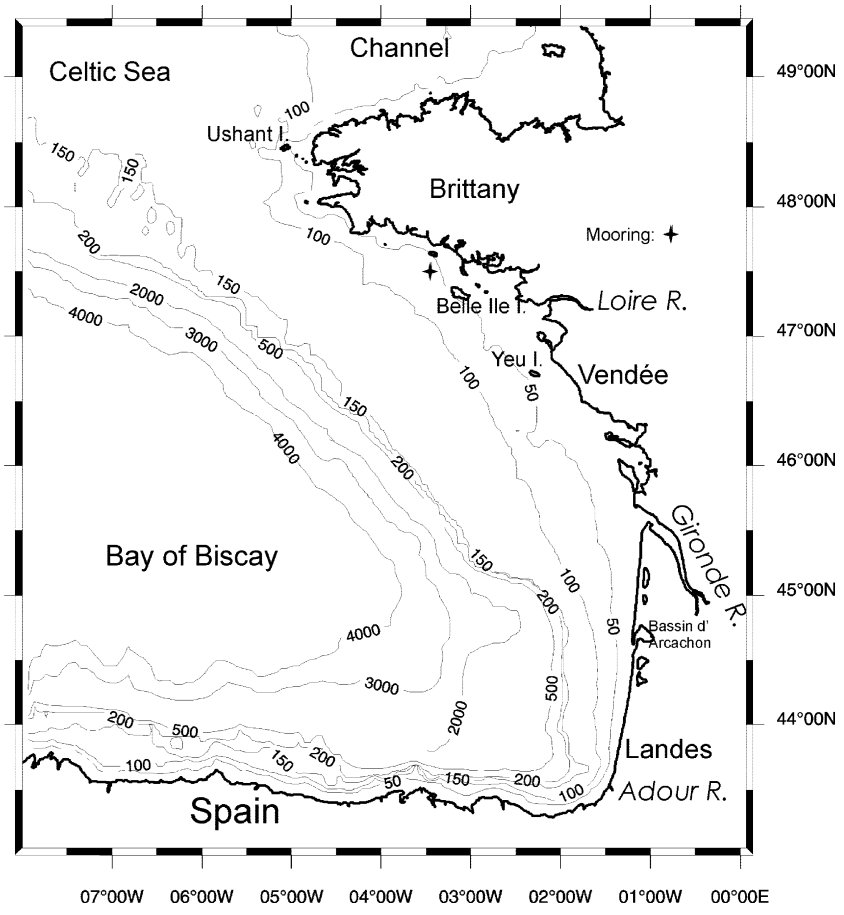

Fig. 3. Model bathymetry.

Huthnance [42], the steep bathymetry at the shelf edge inhibits ocean–shelf exchanges. Moreover, a recent study by Serpette et al. [43] based on lagrangian measurements suggests that the circulation is weak on the outer part of the Armorican shelf and that small anticyclonic eddies prevail. However, this simplification limits the reliability of the model results on the outer shelf and over the shelf break.

The modeled shelf hydrological system is a rather short memory system which recovers from these initial conditions within a year; this makes necessary to simulate a one year spin-up during which the model's outputs might not be relevant. Thus, the results are not analyzed before the beginning of 1997.

5.2. Results

5.2.1. Tidal dynamics

A realistic tidal evolution of the free surface was composed from the eight tidal constituents (M2, S2, K2, N2, 01, K1, P1, Q1) of the Schwiderski atlas [39]. From a one year long simulation, a harmonics analysis was used to extract the main tidal constituents (amplitude and phase) for the 8 waves at each point of the domain. This enabled a comparison with tidal constituents which are well-known in some harbors along the coast (list given in [44]). Comparisons were also made over the entire continental shelf with a recent database (CST France) built by the SHOM [45]. This harmonic database includes 115 constituents and has been built on the basis of a 2D barotropic model adjusted with existing measurements. It covers the continental shelf of the Bay of Biscay and the Channel. The base resolution is 5 km.

Rather than present a comparison with each tidal constituent, we preferred to compute the mean differences in amplitude and time between models and composed the tidal elevation from the CST France database [45]. The period of comparison included two spring–neap cycles (nearly one month). The differences in amplitude and time were calculated as followed:

- At each high tide, the tidal range was computed for both model and CST France harmonical composition.
- The time lag represents the difference of the moments at which the sea surface elevations cross the mean sea level for both model and CST France harmonical composition.

These values were averaged over the month and are presented in Fig. 4a and b.

Please cite this article in press as: Lazure P, Dumas F, An external–internal mode coupling for a 3D hydrodynamical ..., Adv Water Resour (2007), doi:10.1016/j.advwatres.2007.06.010

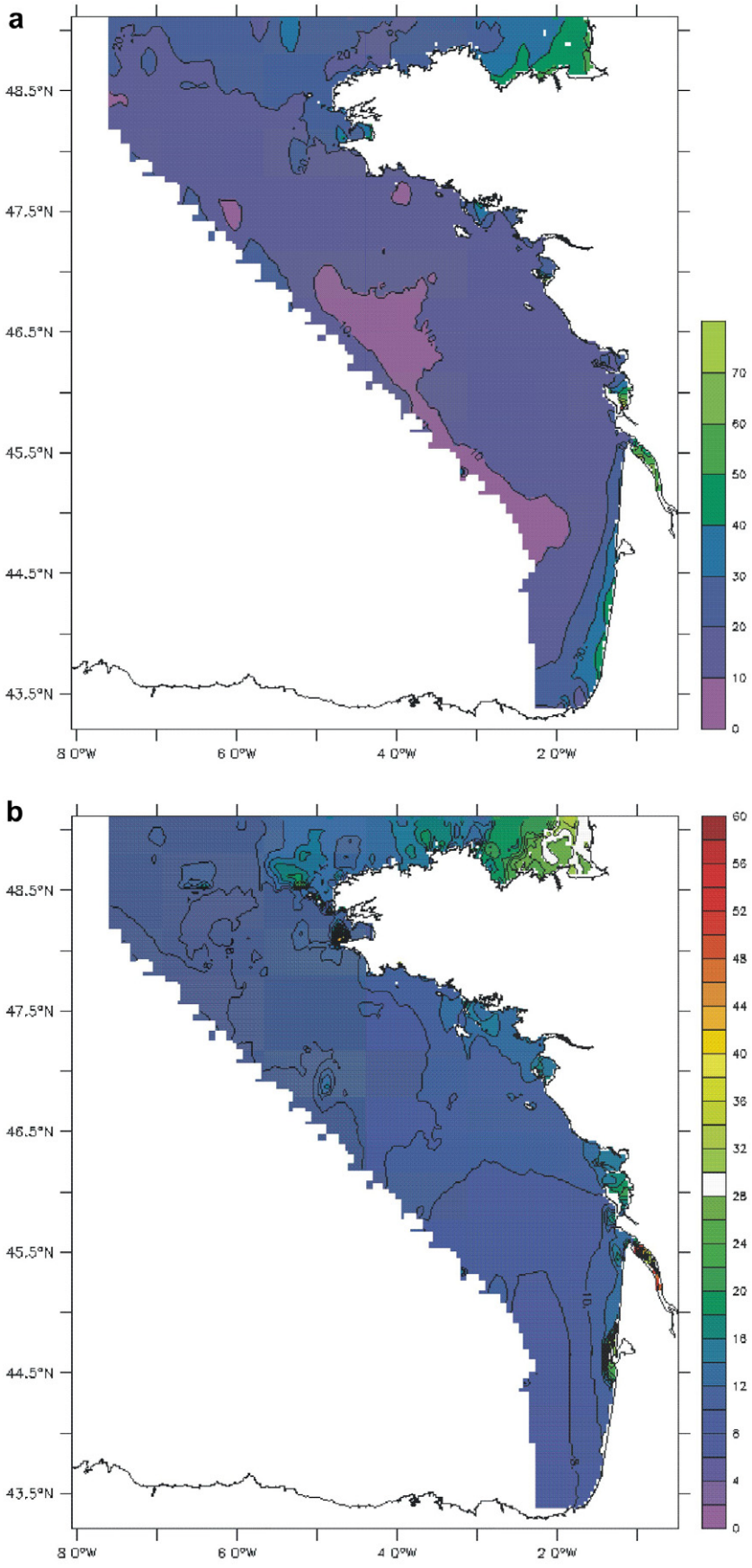

Fig. 4. (a) Averaged differences (in centimeter) between simulated and harmonic reconstruction of tidal levels. (b) Averaged differences in time (in minutes).

Please cite this article in press as: Lazure P, Dumas F, An external–internal mode coupling for a 3D hydrodynamical ..., Adv Water Resour (2007), doi:10.1016/j.advwatres.2007.06.010

The average differences over most of the domain are less than 20 cm (Fig. 4a). The increase in this difference in the Gironde and around the Loire estuaries is due to the mesh size, which cannot accurately describe tidal propagation. This discrepancy does not actually influence hydrodynamics on the shelf. Nevertheless, these differences never reach 20 cm in the Bay of Biscay, contrary to the Channel, especially in the eastern part, where they reach 30 cm. It must be remembered, however, that the tidal ranges increase significantly in the area, reaching 12 m in spring tide. Therefore, the relative precision of the simulation remains constant.

Time differences between model and measurements were lesser than 20 min. over the shelf (Fig. 4b). The increases in time shifts in the southern part of the Bay raise some questions. No reasons for them were found and the data used for this comparison must be examined further. The largest discrepancies are seen in the north-eastern part of the domain.

However, these comparisons of computed and predicted free surface elevations show that the model accurately reproduced the tidal propagation and allowed us to describe tidal currents which have two effects on hydrology: advection and mixing.

5.2.1.1. Tidal currents. The maximum tidal velocities reached at the surface during mean spring tide are presented in Fig. 5a. As noted above, large spatial gradients appeared. In the northern part, they reach 1 ms^{-1} and rise to more than 2 ms^{-1} near Ushant island. Frontal structures created by tidal mixing appear in these areas. Over most of the shelf (i.e., east of 5°W) tidal currents never exceed 0.5 ms^{-1} except close to some bathymetric anomalies (islands, capes, etc.). It is worth noting that the mesh size is too large to properly solve local structures (mostly within coastal areas) where strong currents might be encountered. In fact, the current velocities showed in Fig. 5a may underestimate the actual ones. Two areas on the shelf are characterized by very weak tidal currents: south of Brittany on the western side of Belle Ile and the southern part of the Bay (south of 45°N). Mixing over the main part of the shelf is expected to be weak, allowing thermal stratification from spring to fall and haline stratification due to the plume dynamics.

5.2.1.2. Tidal Eulerian currents. Tidal Eulerian currents were locally averaged during a M2-tidal cycle to evaluate the Eulerian currents (Fig. 5b). Over most of the shelf and the deep part of the Bay of Biscay, the Eulerian currents were extremely weak (less than 1 cm/s). These currents were significantly enhanced wherever non-linearities are higher: close to the coast and around capes and islands. Eulerian currents increased in the northern part of the Bay, west of Brittany. Several gyres generated by the bathymetry appear, where the velocity may reach up to 10 cm/s under average tidal conditions.

5.2.2. Model validation

The comparison of sea surface elevation and the two velocity components at 20 m above the bottom is shown in Fig. 6. We see that the agreement between calculated and simulated elevation is quite good. This period

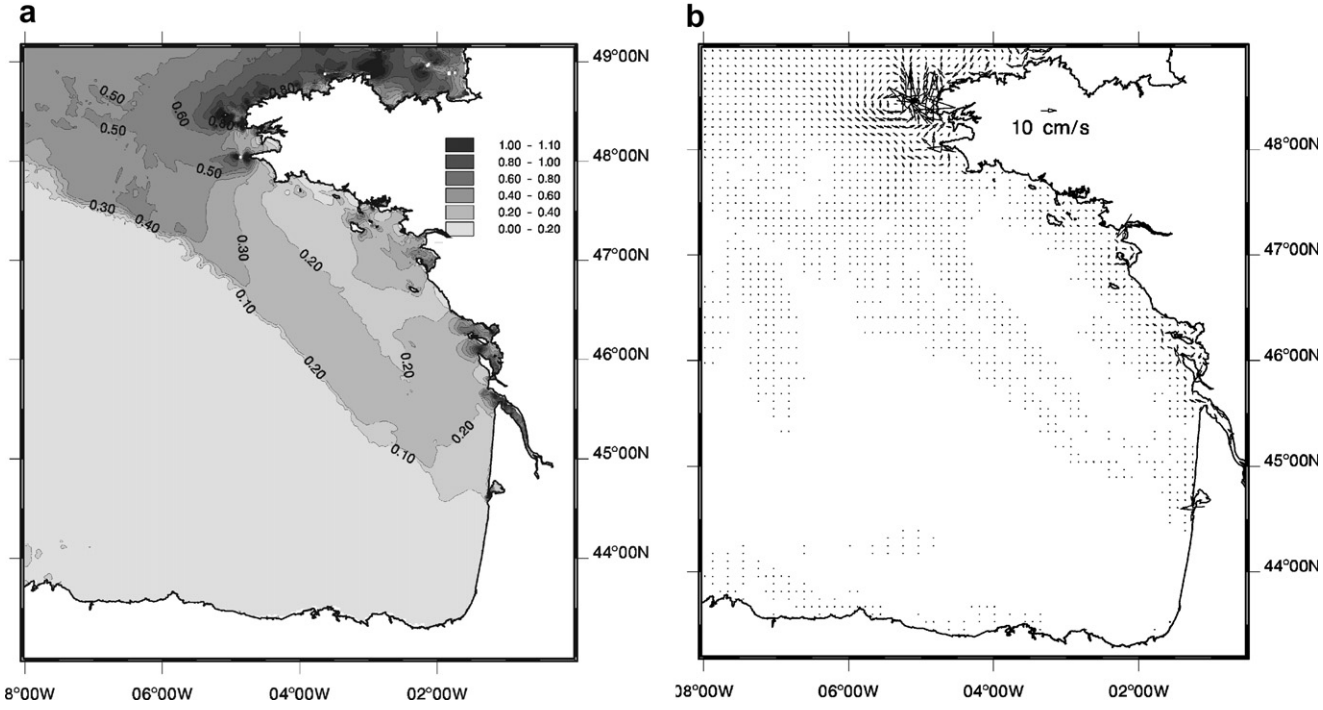

Fig. 5. (a) Maximum velocity during average spring tide. (b) Tidal Eulerian residual current.

Please cite this article in press as: Lazure P, Dumas F, An external–internal mode coupling for a 3D hydrodynamical ..., Adv Water Resour (2007), doi:10.1016/j.advwatres.2007.06.010

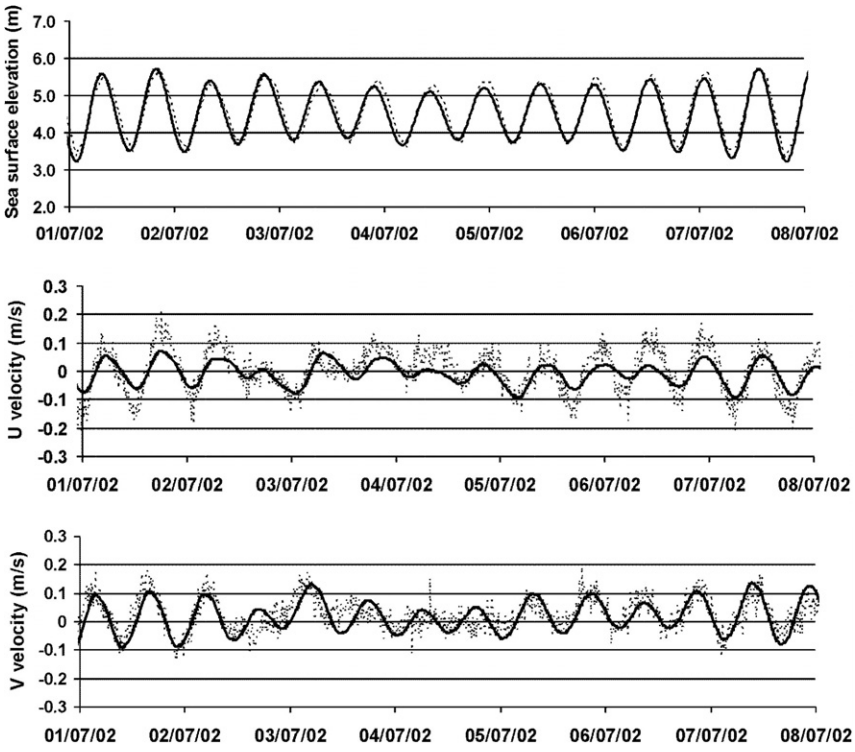

Fig. 6. Model (continuous lines) versus moored ADCP (dotted lines): tidal elevation (top panel), eulerian currents components (mid and bottom panel) over the shelf.

corresponded to neap tides and ended at an average tide. Amplitudes vary from 1.5 to 2.6 m. Differences between the model and observations never reach 5 cm.

Currents are also well reproduced even though they are relatively less accurate. Period with quite small currents, typical of the continental shelf dynamics at this time below the thermocline and the Ekman layer can be seen. Although satisfactory this comparison during a short period needs to be completed by an assessment of the ability in simulating long term (at least seasonal) hydrodynamics like thermal structure or fate of river runoff.

5.2.3. Coastal upwelling

1997 and 1998 were rather dry years: runoffs were significantly weaker than their seasonal climatological values. In June 1997, winds were north-westerly one week before the cruise. As a result, a drop in surface temperature was observed near the coast (Fig. 7). The model shows good agreement with measurements. The bottom temperature was significantly lower than that observed. This discrepancy may be attributed to both the initial conditions which might have been too cold. However, the general features were reproduced properly: the drop in isotherms near the coast, the coastal temperature between 14.5 and 15 °C as showed by measurement, the simulated surface layer thickness of about 30 m and the temperature on the shelf of about 16 °C.

5.2.4. Salinity fields

River runoffs during the winter of 1997–1998 and spring 1998 were slightly weaker than the climatological values.

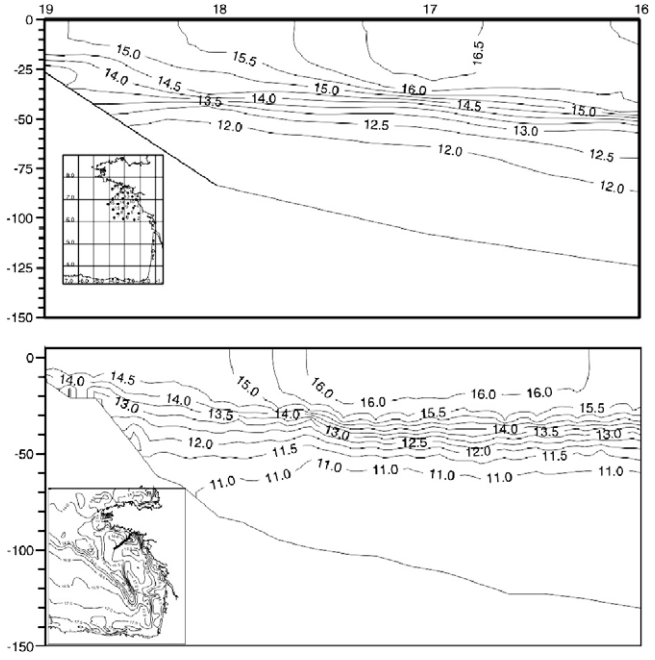

Fig. 7. Temperature transect. (Upper) Modycot 97-1 measurements. Locations of stations are shown on the map of the Bay of Biscay. (Lower) model temperatures. Simulated sea surface temperature is shown in the lower left corner.

During spring, the Loire and Gironde runoffs were about 1100 $m^3 s^{-1}$ and the Adour's was 300 $m^3 s^{-1}$. Winds during the months before the Modycot 98-3 cruise showed a classic evolution. During April, strong winds blew from the

SW. Light north-westerly winds blew in May and the beginning of June was marked by moderate westerly winds. The measured salinity field (Fig. 8) is representative of the fate of Loire and Gironde plumes and the transport by wind and density gradient-induced currents. A strip of salinity of less than 35 extends from the coast to about 100 km offshore in the north, and 40 km offshore in the southern part of the Bay. Off the Loire estuary, salinity decreases and the plume seems to extend southwards, with a strong spatial gradient near Belle Ile island. Off the Gironde estuary, the plume is oriented toward the north. On the Landes coast, the Adour plume ran along the coast. Simulated surface salinity reproduced most of these features. A wider coastal strip of low salinity was also simulated in the north. A discrepancy appeared in the south where the isohaline 35 did not extend along the Landes coast. The Loire plume also showed a southward spreading with a strong gradient near Belle Ile. The offshore extension of the Loire and Gironde plumes correlate well with observations. The vertical structure (Fig. 9) of a transect between southern Brittany and the Gironde estuary showed good agreement. The pycnocline depth was 30 m in both the model and observations. The fresh water under 34.5 psu was the Loire plume. In the Gironde estuary, mixing induced a slant in the isohaline which intersected with the bottom.

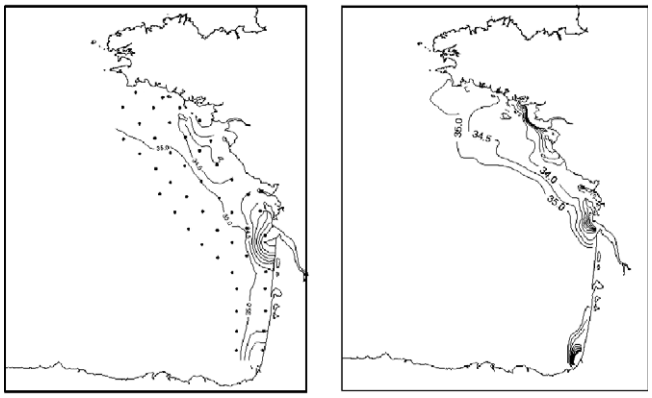

Fig. 8. Measured surface salinity (5 m) during Modycot 98-3 (1998/04/22-27) versus computed surface salinity on 1998/04/26.

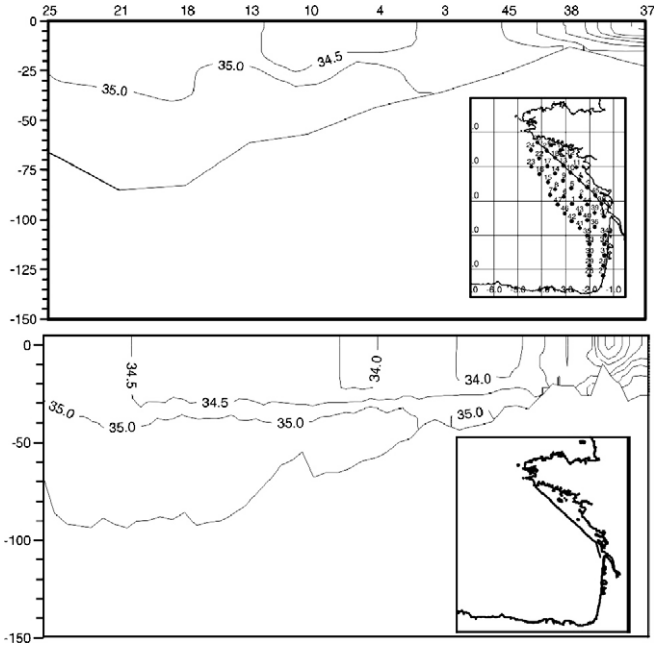

Fig. 9. (Upper) Salinity transect measured during Modycot 98-3 (1998/04/22-27). (Lower) Simulated salinity transect on 1998/04/26.

6. Conclusion

The MARS model presented in this paper aims to describe hydrodynamics from the regional to local scales. It uses a mode splitting method and belongs to the class of 3D models based on a semi-implicit scheme for the external mode which deals with fast motion gravity waves. The use of an ADI scheme for this mode allows a high time step for the external mode which is then of the same order of magnitude of that used for the internal mode, meaning that they can be processed with the same time step.

The main novelty lies in the coupling of these two modes through an iterative predictor–corrector which provides a perfect fit between the barotropic currents and the vertically integrated 3D currents. This removes from the process a post-correction for 3D currents to ensure full consistency between the mean current and vertical integration of 3D currents. Moreover, this fitting this gives to MARS a high stability which is very close to the one of the barotropic model alone.

The stability analysis conducted has shown that the time step criterion to be satisfied is a Courant number (based on current velocity) close to unity. This allows a large time step and makes the MARS model capable of dealing with long-term simulations required for applications, especially those related to biology issues, on the continental shelf. The adaptative time stepping also constitutes a useful procedure to both optimize computation time and enhance robustness.

For most of the other aspects (turbulence closure, vertical coordinates, accounting for rivers) MARS is maintained in the state of the art. The application showed is typical of regional scale applications using MARS, also used in other hydrodynamic environments such as the English Channel [46] and North Sea [47] where tidal processes dominate or in the north-western Mediterranean Sea [48] where mesoscale processes are dominant.

The application to the Bay of Biscay lies in between and is a good test case for 3D models of coastal dynamics, seeing the variety of processes that coexist there. Simulations and measurements correlated in a quite satisfactory manner. Barotropic tides were accurately reproduced and validated the use of semi-implicit time stepping for the external mode in regional scale applications on the order of magnitude of the tidal wave length. A comparison with current

Please cite this article in press as: Lazure P, Dumas F, An external–internal mode coupling for a 3D hydrodynamical ..., Adv Water Resour (2007), doi:10.1016/j.advwatres.2007.06.010

measurements has proven the model's accuracy. At the subtidal time scale, tidal mixing required to investigate hydrology and its variability was validated by comparison with the salinity fields measured. This includes validation of the turbulence closure scheme which gave correct depths for the halocline and the transport scheme which displayed low salinity patches correctly over time and space even after a long time integrated solution.

References

[1] Davies AG. Numerical modelling of stratified flow: a spectral approach. Continental Shelf Res 1982;2:275–300.
[2] Madec G, Delecluse P, Imbard M, Levy C. OPA 8.1 general circulation model reference manual. Notes de l'IPSL no. 11, 1998.
[3] Winton M, Hallberg R, Gnanadesikan A. Simulation of density-driven frictional downslope flow in z-coordinate ocean models. J Phys Oceanogr 1998;28:2163–74.
[4] Bleck R, Smith LT. Wind-driven isopycnic coordinate model of the North and Equatorial Atlantic Ocean 1. Model development and supporting experiments. J Geophys Res 1990;95:3273–85.
[5] Phillips NA. A coordinate system having some special advantages for numerical forecasting. J Meteorol 1957;14:185.
[6] Blumberg AF, Mellor GL. A numerical calculation of the circulation in the Gulf of Mexico, Dynalysis of Princeton, Report no. 66, 1981.
[7] Song YT, Haidvogel D. A semi-implicit ocean circulation model using a generalised topography following coordinate system. J Comput Phys 1994;115:228–48.
[8] Pietrzak J, Jakobson J, Burchard H, Vested HJ, Petersen O. A three dimensional hydrostatic model for coastal and ocean modelling using a generalised topography following coordinate system. Ocean Modell 2002;4:173–205.
[9] Haney RL. On the pressure gradient force over steep topography in sigma coordinate ocean models. J Phys Oceanogr 1991;21:610–9.
[10] Shchepetkin AF, McWilliams JC. A method for computing horizontal pressure-gradient force in an oceanic model with a non-aligned vertical coordinate. J Geophys Res (C Oceans) 2003;108:C3.
[11] Luyten PJ, Jones JE, Proctor R, Tabor A, Tett P, Wild-Allen K. COHERENS: a coupled hydrodynamical-ecological model for regional and shelf seas: user documentation, 1999.
[12] Blumberg AF, Mellor GL. A description of a three dimensional coastal ocean circulation model. In: Heaps NS, editor. Three dimensional coastal ocean models. Coastal and Estuarine science, 4. Washington DC: AGU; 1987. p. 1–16.
[13] Shchepetkin AF, Mc Williams JC. The regional oceanic modelling system (ROMS): a split explicit, free-surface, topography-following-coordinate oceanic model. Ocean Modell 2005;9:347–404.
[14] Blumberg AF. A primer for ECOM-si. Technical report, 1994, Hydroqual Inc., Mahwah NJ, 80pp.
[15] Casulli V, Cheng RT. Semi-implicit finite difference methods for three-dimensional shallow water flows. Int J Numer Methods Fluids 1992;15:15629–48.
[16] Lin B, Falconer A. Three dimensional layer-integrated modelling of estuarine flows with flooding and drying. Estuarine, Coast Shelf Sci 1997;44:737–51.
[17] Cugier P, Le Hir P. Development of a 3D hydrodynamic model for coastal ecosystem modelling application to the plume of the Seine River (France). Estuarine Coastal Shelf Sci 2002;55:673–95.
[18] Ezer T, Arango H, Shchepetkin AF. Developments in terrain-following ocean models: intercomparisons of numerical aspects. Ocean Modell 2002;4:249–67.
[19] Chen X. A fully hydrodynamic model for three-dimensional free-surface flows. Int J Numer Methods Fluids 2003;42:929–52.
[20] Mellor GL. An equation of state for numerical models of ocean and estuaries. J Atmos Oceanic Technol 1991;8:609–11.
[21] Mellor GL, Blumberg AF. Modeling vertical and horizontal diffusivities with the sigma coordinate system. Month Weather Rev 1985;113:1379–83.
[22] Mellor GL, Yamada T. Development of a turbulence closure model for geophysical fluid problems. Rev Geophys Space Phys 1982;20:851–75.
[23] Luyten PJ, Deleersnijder E, Ozer J, Ruddick KG. Presentation of a family of turbulence closure models for stratified shallow water flows and preliminary application to the Rhine outflow region. Continent Shelf Res 1996;16:101–30.
[24] Peaceman DW, Rachford H. The numerical solution of parabolic and elliptic differential equations. J Soc Ind Appl Math 1995;3:28–41.
[25] Leendertse JJ. A water quality simulation model for well-mixed estuaries and coastal seas. Principles of computations. 1970. The rand corporation, RM-6320-RC/1.
[26] Wolf J. A comparison of a semi-implicit with an explicit scheme in a three dimensional hydrodynamical model. Continent Shelf Res 1983;2:215–29.
[27] Leonard BP. A stable and accurate convective modelling procedure based on quadratic upstream interpolation. Comput Methods Appl Mech Eng 1979;19:59–98.
[28] Leonard BP. The ULTIMATE conservative difference scheme applied to unsteady one-dimensional advection. Comput Methods Appl Mech Eng 1991;88:17–74.
[29] Leendertse JJ, Liu SK. A three dimensional model for estuaries and coastal seas. Turbulent energy computation. Rand corporations report R-2187-OWRT. 1977. The Rand Corporation, Santa Monica, CA.
[30] De Goede ED. A time-splitting method for the three-dimensional shallow water equations. Int J Numer Methods Fluids 1991;13:519–34.
[31] Warner JC, Sherwood C, Arango H, Signell R. Performance of four turbulence closure models implemented using a generic length scale method. Ocean Modell 2005;8:81–113.
[32] Blayo E, Debreu L. Adaptative mesh refinement for finite difference ocean model: some first experiments. J Phys Oceanogr 1999;29:1239–50.
[33] Koutsikopoulos C, Le Cann B. Physical processes and hydrological structures related to the Bay of Biscay anchovy. Sci Marina 1996;60:9–19.
[34] Pingree RD, Le Cann B. Celtic and Armorican slope and residual currents. Prog Oceanogr 1989;23:303–38.
[35] Puillat I, Lazure P, Jégou AM, Lampert L, Miller PI. Hydrographical variability on the French continental shelf in the Bay of Biscay during the 1990s. Continent Shelf Res 2004;24:1143–63.
[36] Pingree RD, Mardell GT, Holligan PM, Griffiths GK, Smithers J. Celtic sea and armorican current structure and the vertical distribution of temperature and chlorophyll 'a'. Continent Shelf Res 1982;1:99–116.
[37] Mariette V, Le Cann B. Simulation of the formation of the Ushant thermal front. Continent Shelf Res 1985;4:637–60.
[38] Vrignaud C. Mesures par profileur de courant à effet Doppler de type "ADP 500kHz" Campagnes MODYCOT 2001 et 2002. SHOM Techn. Rep. 2002., No. 227/EPSHOM/CIS/IES.
[39] Schwiderski EW. Ocean tides, Part II: A hydrodynamical interpolation model. Mar Geodes 1980;3:219–55.
[40] Luyten PJ, De Mulder T. A module representing surface fluxes of momentum and heat. 1992. Technical report No 9 MAST-0050-C.
[41] Reynaud T, Legrand P, Mercier H, Barnier B. A new analysis of hydrographic data in the Atlantic and its application to an inverse modelling study. Int WOCE Newsletter 1998;32:29–31.
[42] Huthnance JM. Circulation, exchange and water masses at the ocean margin: the role of physical processes at the shelf edge. Prog Oceanogr 1995;35:353–431.
[43] Serpette A, Le Cann B, Colas F. Lagrangian circulation of the North Atlantic Central Water over the abyssal plain and continental slopes of the Bay of Biscay: description of selected mesoscale features. Sci Marina 2006;70s1:27–42.

Please cite this article in press as: Lazure P, Dumas F, An external–internal mode coupling for a 3D hydrodynamical ..., Adv Water Resour (2007), doi:10.1016/j.advwatres.2007.06.010

[44] Le Cann B. Barotropic tidal dynamics of the Bay of Biscay shelf: observations, numerical modelling and physical interpretation. Continent Shelf Res 1990;10:723–58.

[45] Le Roy R, Simon B. Réalisation et validation d'un modèle de marée en Manche et dans le Golfe de Gascogne. Application à la réalisation d'un nouveau programme de réduction des sondages bathymétriques. Techn. Rep. 2003. EPSHOM no. 002/03.

[46] Bailly du Bois P, Dumas F. Fast hydrodynamic model for medium- and long-term dispersion in seawater in the English Channel and southern North Sea, qualitative and quantitative validation by radionuclide tracers. Ocean Modell 2005;9:169–210.

[47] Delhez E, Damm P, de Goede E, de Kok JM, Dumas F, Gerritsen H, et al. Variability of shelf-seas hydrodynamic models: lessons form NOMADS2 project. J Marine Syst 2004;45:39–53.

[48] André G, Garreau P, Garnier V, Fraunié P. Modelled variability of the sea surface circulation in the North western Mediterranean Sea in the Gulf of Lions. Ocean Dyn 2005;55:294–308.

Please cite this article in press as: Lazure P, Dumas F, An external–internal mode coupling for a 3D hydrodynamical ..., Adv Water Resour (2007), doi:10.1016/j.advwatres.2007.06.010